

COVER PAGE

Document downloaded by @DAEL

Sat Nov 28 12:46:38 2026
For personal use

When automatic English translation is provided, only the original document is authentic.
The EAA cannot be held responsible of any translation error

Bibliographical reference

Propagation Behavior of Lamb Waves in Functionally Graded Piezoelectric Plates, Morched Ben Amor, Issam Ben Salah and Mohamed Hédi Ben Ghozlen, Acta Acustica **vol. 101** (Number 3), 2015, pp. 435-442

DOI
https://doi.org/10.3813/AAA.918839

Acta Acustica united with Acustica
Vol. 101 (2015) 435 – 442

Review Article
DOI 10.3813/AAA.918839

Propagation Behavior of Lamb Waves in Functionally Graded Piezoelectric Plates

Morched Ben Amor[1)], Issam Ben Salah[2)], Mohamed Hédi Ben Ghozlen[2)]
[1)] Institut Préparatoire aux Études des ingénieurs de Sfax, Route Menzel Chaker Km 0.5, Sfax, Tunisie.
morchedbenamor@gmail.com
[2)] Laboratoire de Physique des Matériaux, Faculté des Sciences de Sfax, B.P.1171, 3018 Sfax, Tunisia.

Summary
The propagation of lowest-order symmetric (S_0) and anti-symmetric (A_0) Lamb wave modes in a functionally graded piezoelectric material (FGPM) is investigated. The electromechanical material properties change continuously with the thickness of the layer with exponential variation. The first-order differential equations are solved by Peano-Series method. A comparative study has been carried with the ordinary differential equation (ODE). A good agreement is observed between the two methods. The influence of the gradient coefficients of the FGPM on the dispersion curves and the electromechanical coupling factor are investigated. Further, the effect of polarization direction on the electromechanical coupling factor is also illustrated.

PACS no. 43.20.-f

1. Introduction

With the development of the material technology, the functionally graded piezoelectric materials (FGPM) are manufactured. To improve the efficiency and natural like of the SAW devices, FGPM is considered to apply in SAW devices [1, 2, 3, 4]. Hence, the research of waves propagation behaviors and characteristics in FGPM has become a topic of particular interest and importance. In recent years there has been a growing interest in using Lamb waves for a variety of physical sensors [1, 4, 5, 6, 7]. Important advantages over SAW sensors are obtained by utilizing the lowest-order anti-symmetric Lamb wave mode (A_0) propagating in plates that are only a few micrometers thick [2].

For Lamb waves propagating in inhomogeneous medium for which the electromechanical materials parameters vary continuously, analytical solutions can be obtained only for some special cases, due to the complexity of the governing equations. Hence, a variety of different numerical procedures have been used to study the propagation waves in functionally graded piezoelectric material (FGPM). By applying the hybrid numerical method, Liu *et al.* [5] investigated surface waves propagating in FGM plate. These methods, if used for FGM plates, make it necessary to divide the graded structure into sub-layers of averaged properties in the direction of compositional gradation. However, these studies all dealt with the material properties of laminated plates, which were homogeneous within each layer.

Received 01 June 2014,
accepted 13 November 2014.

Recently, resonant Lamb wave based geometries on c-oriented Aluminum nitride (AlN) thin film membranes were studied [3, 4, 5]. Attention has been focused on the lowest order symmetric (S_0) Lamb mode because of its extremely high velocity compared to the anti- symmetric (A_0) mode, thus being suitable for high frequency applications [3, 5, 6].

In the present contribution, we analyzed the propagation of lowest-order (S_0) and (A_0) Lamb wave modes in aluminum nitride plates (AlN). We here assume that all electromechanical material properties have the same exponential function distribution along the depth direction. The first-order differential equations are solved by Peano-Series method [8, 9, 10]. The influence of the gradient variation of material constants on dispersion curves and the coupled electromechanical factor is carried out.

2. Theoretical background

Let us consider a generally anisotropic medium (Figure 1) and a harmonic wave propagating along the x-axis of the form $\eta(z)\exp[\mathrm{i}(\omega t - k_1 x)]$, where k_1 is the horizontal wave number, ω is the angular frequency. The origin of the Cartesian coordinate system (x, y, z) is set on the surface with the z-axis pointing into the plates faces, and it is assumed to be the symmetry of the medium. The polarization direction of the piezoelectric material is parallel to the z-axis, and the material properties change gradually with depth.

The normal stress vector $\tau_{i3} = [\tau_{13}, \tau_{23}, \tau_{23}]$ and the particle displacement $u = [u_1, u_2, u_3]$ are chosen as the six mechanical variables. The wave equation for displacement field is a second order differential equation with varying

© S. Hirzel Verlag · EAA

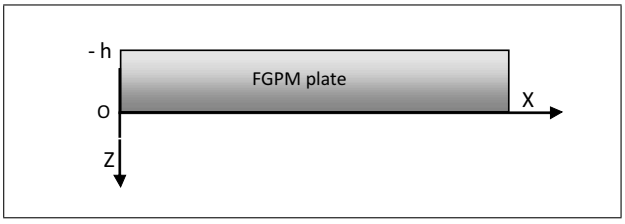

Figure 1. FGPM plate and Cartesian coordinates.

coefficients for which no explicit analytical solution generally exists unless appropriate profiles are involved allowing some special functions representation of the wave field.

It is well known that elastic and electric excitation in a piezoelectric media are interconnected and can be described in a quasi-static approximation by the following governing field and the equations without body forces and free charges and the constitutive relations

$$\rho\ddot{u}_j = \tau_{ij,j}, \qquad D_{i,i} = 0, \tag{1}$$

$$\tau_{ij} = C_{ijkl}u_{k,l} + e_{lij}\phi_{,l}, \quad D_i = e_{ikl}u_{k,l} - \varepsilon_{il}\phi_{,l}, \tag{2}$$

where u_j are the mechanical displacement components, ϕ the electrical potential function, ρ the density. Also τ_{ij} and D_i are the stress and electric displacement field, C_{ijkl}, e_{lij}, ε_{il} are the elastic, piezoelectric and the dielectric constants, respectively.

To describe the Lamb waves in the FGPM plate, the following boundary and continuous conditions should be satisfied. Both surfaces of the plate $z = 0$ and $z = -h$ [1, 2],

$$\text{Electric shorted circuit: } \phi = 0 \text{ and } \tau_{i3} = 0 \quad (i = 1, 3). \tag{3}$$

$$\text{Electric open circuit: } \quad \sigma = 0 \text{ and } \tau_{i3} = 0 \quad (i = 1, 3). \tag{4}$$

σ refers to the charge density, it can be deduced from D_3 (the normal electric displacement) values in the neighborhood of free surfaces,

$$\sigma = D_3(-h^+) - D_3(-h^-), \tag{5}$$

$$\sigma = D_3(0^+) - D_3(0^-). \tag{6}$$

In order to deal with the exact problem, that is to keep the continuity of the properties variation, the wave equation is written under the Ingebrigsten and Tonning formalism [11, 12]. The differential equations written in a matrix form reveal a system of first-order with non-constant coefficients [7, 8]:

$$\frac{\mathrm{d}}{\mathrm{d}z}\eta(z) = Q\,\eta(z). \tag{7}$$

The generalized stress-vector $\eta(u_1, u_3, \phi, \tau_{13}, \tau_{33}, D_3)$ includes mechanical stress vector τ_{i3} and the normal electrical displacement D_3. In the same way, the generalized displacement vector includes the mechanical displacement u and the electrical potential ϕ. Q is the fundamental acoustic tensor, a (6×6) matrix function of material properties, wave number and frequency. The fundamental acoustic tensor Q for a piezoelectric medium can be written as [12, 13]

$$Q(z) = \begin{pmatrix} -k_1\gamma_{33}^{-1}\gamma_{31} & -\mathrm{j}\gamma_{33}^{-1} \\ -\mathrm{j}(\gamma_{11}\gamma_{33}^{-1}\gamma_{31})k_1^2 + \mathrm{j}\rho\omega^2 I' & -k_1\gamma_{33}^{-1}\gamma_{31} \end{pmatrix}. \tag{8}$$

I' is the 6×6 identity matrix, ρ is the density of the solid and the 6×6 matrices γ_{ik} are related to the elastic constants C_{ijkl}, piezoelectric constants e_{ijk} and dielectric permittivity constants ε_{ij} by

$$\gamma_{ik} = \begin{bmatrix} C_{1i1k} & C_{1i2k} & C_{1i3k} & e_{k1i} \\ C_{2i1k} & C_{2i2k} & C_{2i3k} & e_{k2i} \\ C_{3i1k} & C_{3i2k} & C_{3i3k} & e_{k3i} \\ e_{i1k} & e_{i2k} & e_{i3k} & -\varepsilon_{ik} \end{bmatrix}. \tag{9}$$

The basic equations (1)–(4) are reformulated with respect to the state vector $\eta(z)$. This vector dimensioned to 6, includes mechanical and electrical components. The procedure aims two things, first the differential equations are transformed into an eigen value equation, second all components are suitable for writing boundary conditions.

3. The Series-Peano method

The Lamb wave propagation (equation 10) is derived from the set of the basic equations (1)–(4), for which an analytical solution exists based on the concept of state-vector and matricant [8, 9]. The matricant $M(z, z^{(0)})$ is the fundamental solution of equation (7) with property

$$\eta(z) = M(z, z^{(0)})\,\eta(z^{(0)}), \tag{10}$$

where $z^{(0)}$ is a reference point on the z-axis.

This analytical solution can be evaluated exactly because the integral increment has been chosen very small. The Matlab software offers the possibility to calculate accurately the Peano-series expansion [8, 9],

$$M(z, z^{(0)}) = I + (\mathrm{i}\omega)\int_{z^{(0)}}^{z} Q(\zeta)\,\mathrm{d}\zeta + (\mathrm{i}\omega)^2\int_{z^{(0)}}^{z} Q(\zeta)\left(\int_{z^{(0)}}^{z} Q(\zeta_1)\,\mathrm{d}\zeta_1\right)\mathrm{d}\zeta + \ldots, \tag{11}$$

where I is the identity matrix of dimension (6,6). The components of the matrix Q are continuous in z-direction and the study interval is bounded (thickness of the waveguide), consequently the hypothesis is always verified.

Using the matricant property through the plate-thickness, the state-vector (defined in equation 11) at the second interface $\eta(0)$ is evaluated from the state-vector at the first interface $\eta(-h)$ as follows [10, 12]: $\eta(0) = M(0, -h)\eta(-h)$. Two cases must be distinguished, electrically shorted (sc) and open (oc) circuit for which the state vector from electrostatic considerations does not keep the same components [8]. For the "sc" case includes the electrical potential ϕ and for the "oc" case $\eta(z)$ includes the charge density σ.

$$\begin{pmatrix} U \\ T \end{pmatrix}_0 = \begin{pmatrix} M_{11} & M_{12} \\ M_{21} & M_{22} \end{pmatrix}\begin{pmatrix} U \\ T \end{pmatrix}_{-h}. \tag{12}$$

For commodity calculations, the matricant M is divided into four blocks: $M_{11}, \ldots, M_{22}$. For both electrical polarizations, (6×6) characteristic matrices M_{sc} and $M_{0\mathrm{c}}$ are then constructed,

$$\begin{pmatrix} u_1 \\ u_3 \\ \sigma \\ \tau_{13} \\ \tau_{33} \\ \phi \end{pmatrix}_0 = \big(M\big)_{\mathrm{sc}} \begin{pmatrix} u_1 \\ u_3 \\ \sigma \\ \tau_{13} \\ \tau_{33} \\ \phi \end{pmatrix}_{-h} \quad \text{Electric shorted circuit,} \quad (13)$$

$$\begin{pmatrix} u_1 \\ u_3 \\ \phi \\ \tau_{13} \\ \tau_{33} \\ \sigma \end{pmatrix}_0 = \big(M\big)_{\mathrm{oc}} \begin{pmatrix} u_1 \\ u_3 \\ \phi \\ \tau_{13} \\ \tau_{33} \\ \sigma \end{pmatrix}_{-h} \quad \text{Electric open circuit.} \quad (14)$$

Specifically, the dispersion equations (13)–(14) for the plate for both cases has non-trivial solutions when the determinant $(M_{21})_{\mathrm{sc,oc}} = 0$. Consequently, to seek out the zeros of $\det(M_{21})$ corresponds to find the couples of values (k_1, ω) which describe the dispersion curves.

4. Numerical results and discussion

To calculate the dispersion curves, we evaluate numerically the matricant $M(z, z^{(0)})$ from the expression (11). This step requires to truncate the Peano series and to numerically calculate the integrals. Thus, the error can be estimated and controlled [10]. For the calculations in the plate we retained 10 terms in the series and evaluate the integrals over 50 points. These choices are not optimized, but to ensure the convergence of the solution and the precision of the results in the range of non-dimension wave number kh considered for a reasonable calculation time.

The propagation behavior of Lamb waves in FGPM plates is studied by the Peano series method. In the case presented here the plate is made of c-oriented AlN with properties materials are given by Table I [3, 5]. $\varepsilon^0 = 8.85 \cdot 10^{12}$ F/m is the dielectric constant of vacuum. In this study all the material properties of the FGPM plate are assumed to vary continuously along the thickness with the exponential distribution

$$\Gamma = \Gamma^{(0)} \exp\big(\beta z\big), \quad (15)$$

where β is the graded coefficient characterizing the degree of the material gradient in the z-direction and the superscript 0 is attached to indicate the z-direction factors in the material coefficients. The subscript 0 and $\beta = 0$ are obvious and correspond to the homogenous material case.

4.1. Effect of the gradient coefficient on phase velocity

To validate the Peano-series method, a known input data has been chosen in order to compare our numerical implementation with the results available in the literature [4].

Table I. Properties of AlN with symmetry hexagonal.

Elastic constants C^0_{ij} (10^{11} N/m^2): $C^0_{11} = 3.45$, $C^0_{12} = 1.25$ $C^0_{13} = 1.2$, $C^0_{33}3.95$, $C^0_{44} = 1.18$, $C^0_{66} = 1.1$
Piezoelectric constants e^0_{ijk} (C/m^2): $e^0_{15} = e^0_{24} = -0.48$, $e^0_{31} = e^0_{32} = -0.58$, $e_{33} = 1.55$
Dielectric constants ε^0_{ij} (10^{11} F/m): $\varepsilon^0_{11} = \varepsilon^0_{22} = 8$, $\varepsilon_{33} = 1.18$
Density $\rho = 3260$ kg/m^3

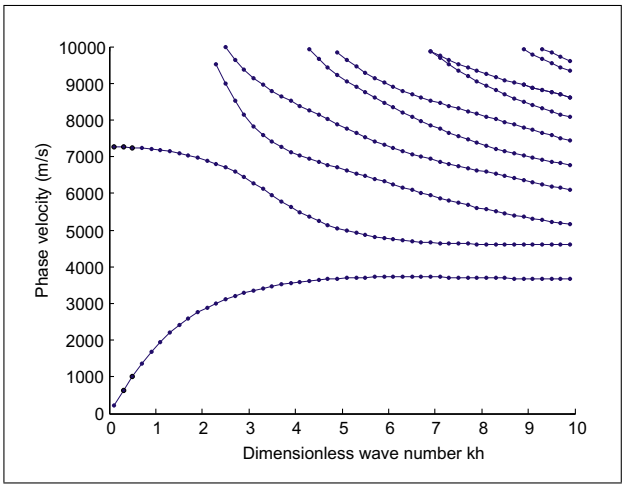

Figure 2. Dispersion curves obtained for FGM plate obtained by power series technique [2] (solid line) and author's result (dotted line).

Therefore, we used a composite made by chrome (Cr) and ceramics materials. The characteristic properties of Cr and ceramic material have been given in [4]. Here, the volume fraction varies linearly in the FGM. Figure 2 presents the dispersion curves obtained by Peano Series method and Power Series Technique [4]. We plotted the dispersion curves vs. kh product ranging from 0 to 10 and the velocity is lower than 10000 m/s. It can be seen (see Figure 2) that for each mode of the lamb wave phase velocities, the numerical results obtained by Peano series method agree with those obtained by power series technique [4].

Furthermore, to illustrate convergence, we consider a relatively simple problem, which is the Lamb waves propagating in homogeneous plate i.e. when the gradient coefficient $\beta = 0$. The piezoelectric material (AlN) is polarized along the z-axis direction.

Figure 3 presents the dispersion curves of the lowest-order symmetric (S_0) and anti-symmetric (A_0) Lamb wave waves propagating in the homogeneous piezoelectric plate obtained by the Peano-series method and ordinary differential equation method [7]. Figure 3 shows a good agreement between the results obtained by the two methods. We note that as non-dimensional wave number increases, the A_0 and S_0 modes velocities tend asymptotically to the V_0: the open Rayleigh velocity. Further, it can

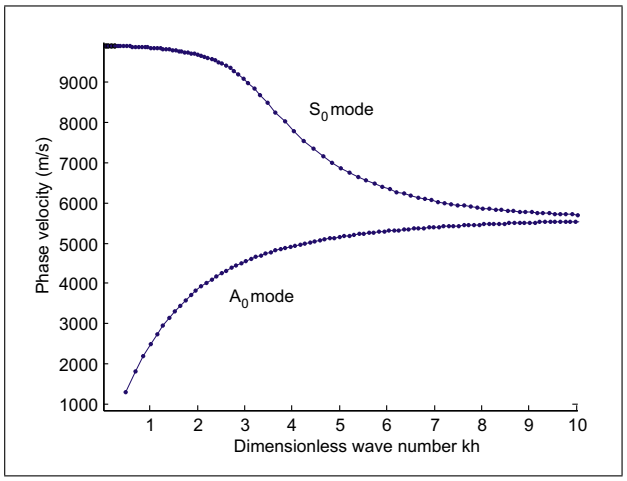

Figure 3. Dispersion curves of S_0 and A_0 Lamb waves modes propagating in AlN homogeneous plate obtained by peano-series (solid line) and ODE methods [7] (point line).

be shown that in thick plates, the surface acoustic wave is essentially obtained by a superposition of the A_0 and S_0 Lamb wave modes.

For surface acoustic waves devises, a high electromechanical coupling factor of the wave is expected in engineering applications. The electromechanical coupling factor for surface waves is defined as [1, 2, 3, 4, 5, 6, 7]

$$K^2 = 2\frac{|V_o - V_c|}{V_o}, \tag{16}$$

where V_o (open) and V_c (shorted) are the phase velocities of the lamb mode for the electrically open and shorted circuits, respectively. This parameter is directly related to the efficiency of the transducer in converting electrically energy to mechanical energy or vice versa.

To show the effect of gradient coefficient on the phase velocity, the variation of the phase velocity versus the frequency is plotted under various gradient coefficient values for electrically open cases. Figure 4 shows the effect of gradient factor on phase velocity of the S_0 mode for the electrically open case as function of non-dimensional wave number kh. It can be seen that the starting value of the phase velocity decreases with an increase frequency but the phase velocity increases with an increase of gradient factor. Besides, the non-dispersive bearing of phase velocity increases when the gradient factor increases. Figure 5 displayed the relative velocity shift $\Delta V/V$ as function of non-dimensional wave number, for the S_0 mode. With the increase of the frequency the minimum of $\Delta V_{co}/V_{co}$ occurs at a higher coefficient gradient factor "β". The obtained curves reveal a minimum for the velocity shift appears at $kh = 4.3$. This minimum moves to the high frequency when the gradient factor β increases.

The electromechanical coupling factor is presented by Figure 6. It can be found that the electromechanical coupling factor of the S_0 mode decreases with the increase of the gradient factor β. The maximum value of the electromechanical coupling factor of the FGPM plate is obtained for the homogeneous piezoelectric plate. Also the

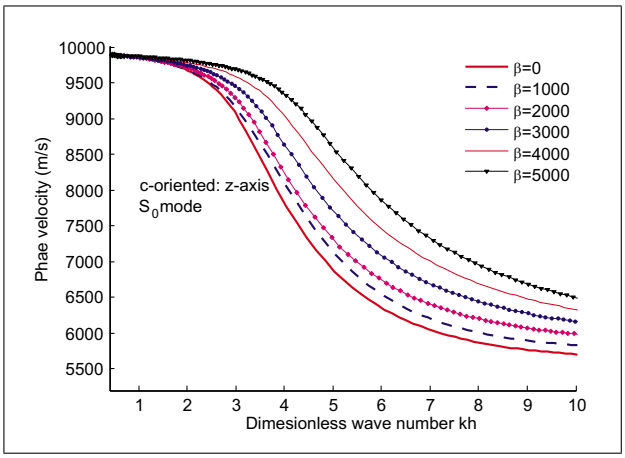

Figure 4. Effect of gradient coefficient on the dispersion curves of S_0 mode for open circuit.

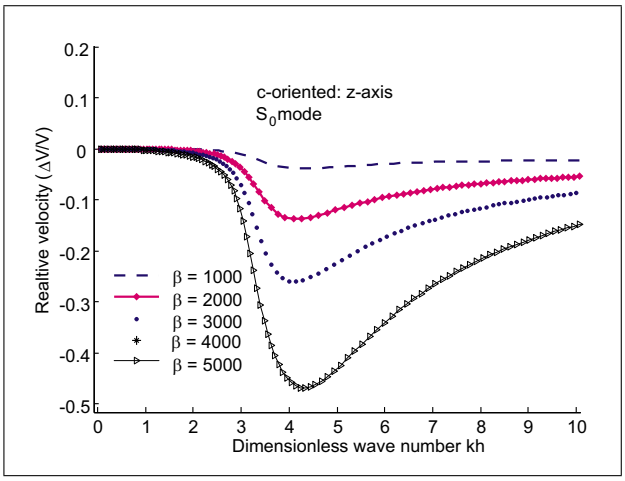

Figure 5. Effect of gradient coefficient on the phase velocity shift for S_0 mode for open circuit.

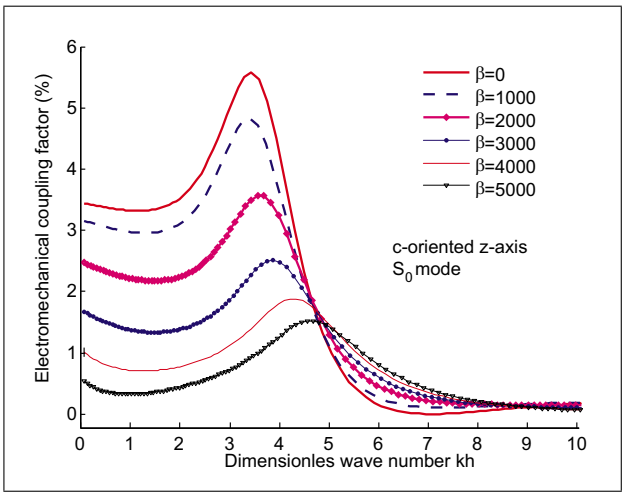

Figure 6. Effect of gradient coefficient on electromechanical coupling factor for S_0 mode for the electrically open circuit.

peak propagation of the electromechanical coupling factor shifts to the high frequency area with an increase in the magnitude of the gradient coefficient, which can be used

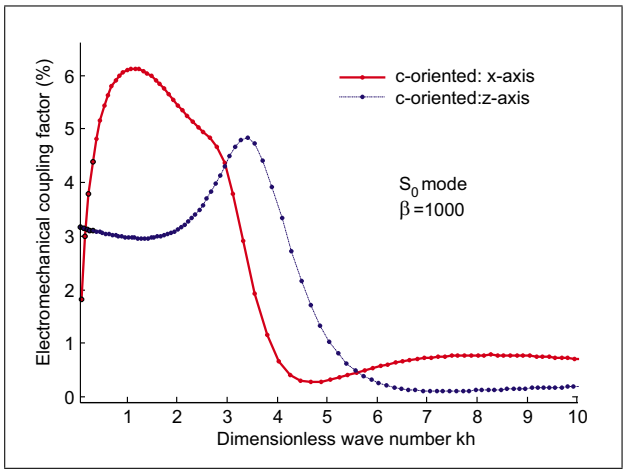

Figure 7. Electromechanical coupling factor of S_0 mode at $\beta = 1000$, solid line: polarization is oriented with x-axis, dashed line: polarization is oriented with z-axis.

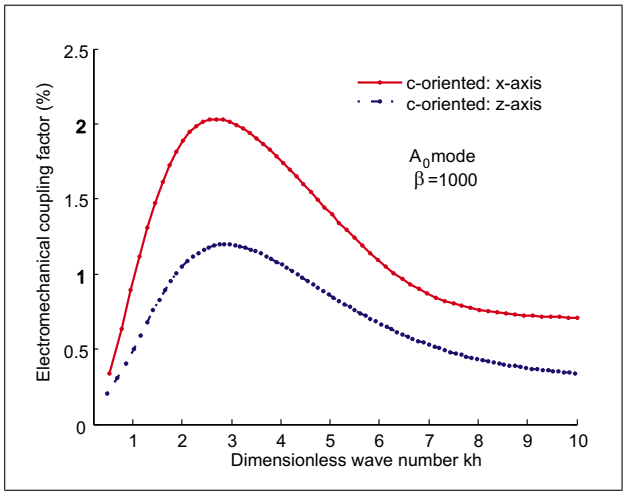

Figure 8. Electromechanical coupling factor of A_0 mode at $\beta = 1000$, solid line: polarization is oriented with x-axis, dashed line: polarization is oriented with z-axis.

to design different SAW sensors with high performance working at different frequencies by adjusting the extent of the gradient properties. However, the starting value of the electromechanical coupling factor decreases with the increases of the magnitude of the gradient coefficient. All the electromechanical tend to the same value when the frequency becomes sufficiently large. This means that the gradient coefficient has an insignificant influence on the energy propagation of the Lamb wave in the ultrahigh frequency zone.

4.2. Influence of piezoelectric axis on the electromechanical coupling factor

In order to investigate the influence of the piezoelectric axis on the electromechanical coupling factor, we have adopted two settings, first the AlN piezoelectric axis has been put along x-axis denoted (parallel configuration), and secondly the piezoelectric axis along the z-axis (vertical configuration). Figure 7 and Figure 8 associated with A_0 and S_0 respectively, reveal the influence of the polarization direction on the electromechanical coupling factor. Both configurations are superimposed on the same figure. Arbitrarily the gradient factor has been fixed $\beta = 1000$. For S_0 mode, the maximum of the electromechanical coupling factor undergoes a sharp enhancement in the low frequency range (kh close to 1). For the A_0 mode the electromechanical coupling factor also undergoes a sharp increase near $kh = 2.8$. The parallel configuration is generally associated with higher electromechanical coupling factor, it slightly exceeds 6% for S_0 and 2% for A_0. Whereas the vertical configuration reveals a dominant electromechanical coupling factor only in the case of S_0 in the area comprised between $kh = 3$ and $kh = 5.5$.

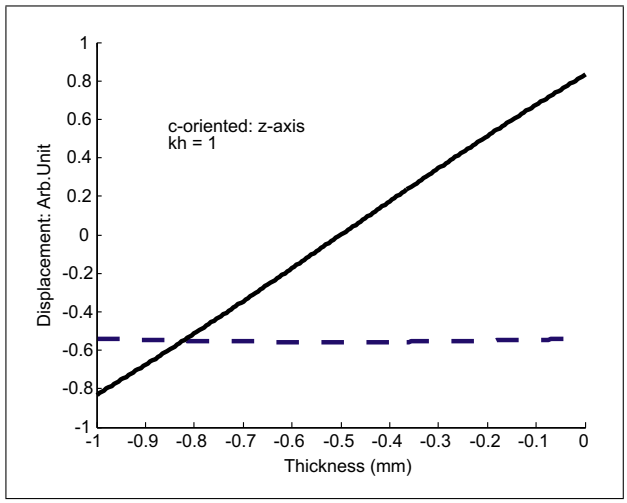

Figure 9. Displacement of the S_0 mode at $kh = 1$for the electrically open circuit, polarization is oriented with z-axis.

4.3. Wave structure analysis

This section highlights the effect of piezoelectric axis on the distributions of some physical quantities through thickness. The significant variations of the electromechanical coupling factor in function of the piezoelectric axis can be explained by analyzing the mechanical or electric profile at the level of different points of the dispersion curve. Therefore, the development of the Peano-series method permits by using the matricant concept, to compute mechanical and electrical amount vs. the plate thickness.

Figures 9–15 are selected to describe how the mechanical and electrical magnitudes vary through thickness for S_0 mode at $kh = 1$. For the vertical configuration, Figure 9 and 10 show that the in-plane displacement u_1 varies along the thickness direction in a nearly symmetric manner with respect to the middle surface, while the vertical displacement u_3 (deflection) changes along the thickness direction in a nearly anti-symmetric manner. In the same way, the parallel configuration leads to a higher and symmetric u1 amplitude, compared with the vertical configuration (see Figures 11a,b). That seems coherent with predominance of the corresponding electromechanical coupling factor. Additionally, from Figure 12 and Figure 13, both components

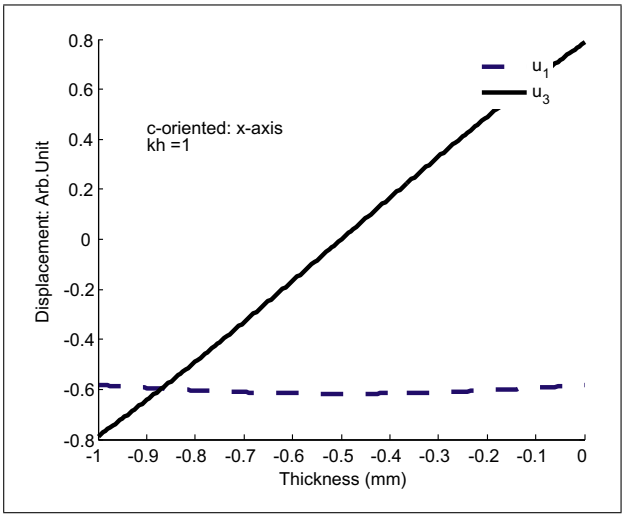

Figure 10. Displacement of the S_0 mode at $kh = 1$ for the electrically open circuit, polarization is oriented with x-axis.

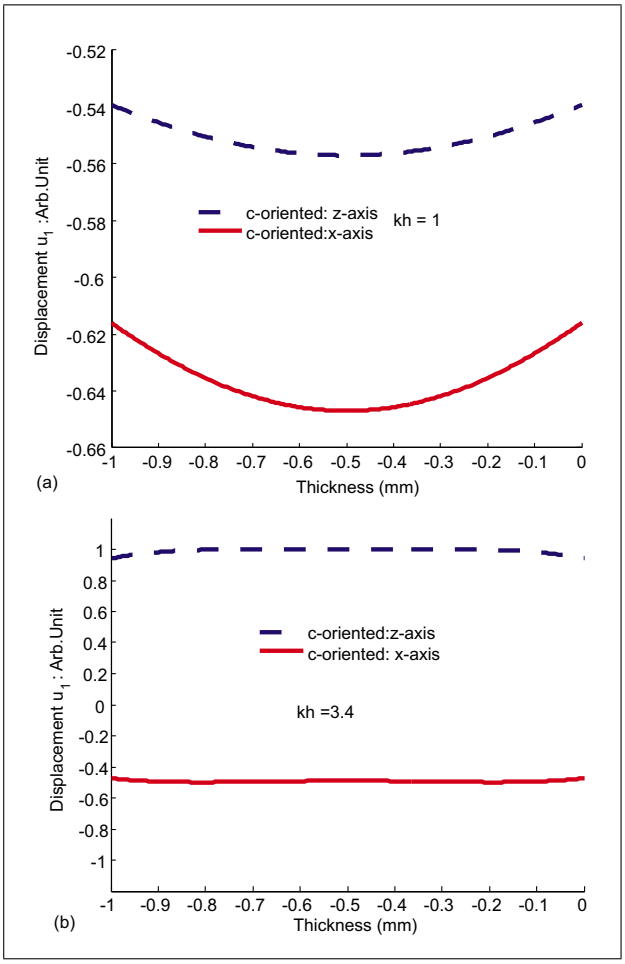

Figure 11. Displacement u1of the S_0 mode for the electrically open circuit, (a) kh =1 and (b) kh =3.4, poplarization along x-axis (solid line), poplarization along z-axis (dashed line).

(τ_{13}, τ_{33}) vanish on the free surfaces, which is compatible with the mechanical boundary conditions. For the area where the coupling factor associated with the vertical configuration becomes predominant, contrary to the previous

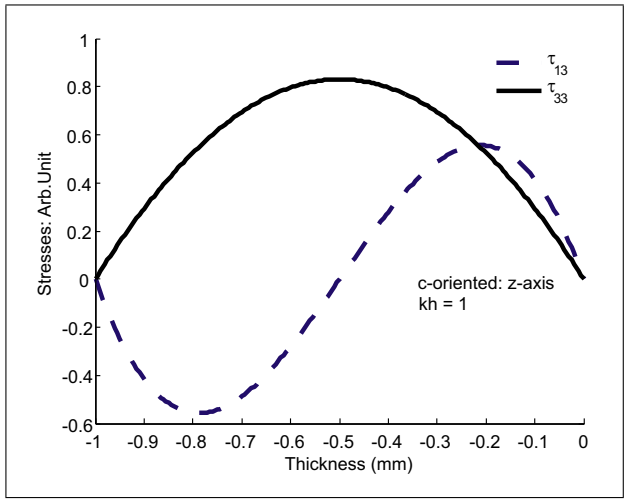

Figure 12. Stresses of the S_0 mode at $kh = 1$ for electrically open circuit, polarization along z-axis.

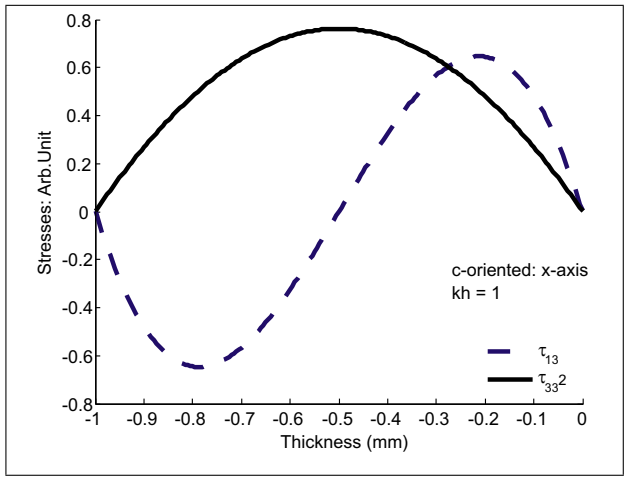

Figure 13. Stresses of the S_0 mode at $kh = 1$ for electrically open circuit, polarization along x-axis.

case the third displacement component u_3 is symmetrical and reinforces the coupling (see Figures 14a,b).

Finally, Figures 15a,b show the profile of electric potential of the S_0 mode: (a) at $kh = 1$ and (b) at $kh = 3.4$ in the case of electrically shorted circuit. At $kh = 1$, for vertical configuration, the potential varies along the thickness direction in a nearly symmetric manner, while the vertical configuration changes along the thickness direction in a nearly anti-symmetric manner. When $kh = 3.4$ there is a change in the symmetry of profile as seen previously, which justify the predominance of electromechanical coupling factor in each case.

5. Conclusions

The Peano-Series method, which gives good convergence and high precision, is employed for solving the problem of Lamb waves that propagate in an FGPM plate, consisting of AlN. This method permits to assess the solution through a more realistic approach without using a multilayer mod-

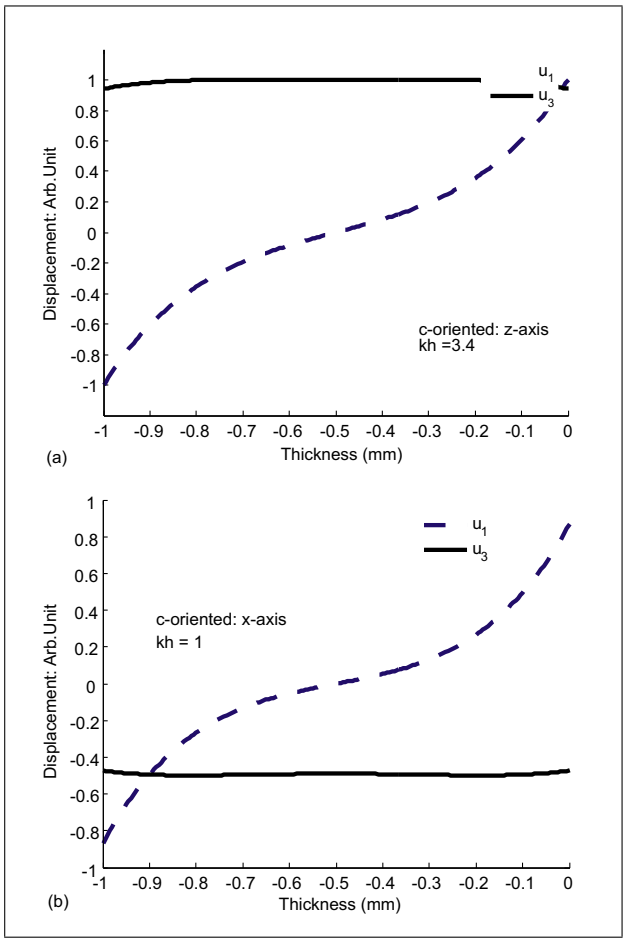

Figure 14. Displacement of the S_0 mode at $kh = 3.4$ for the electrically open circuit, (a): polarization along z-axis and (b): polarization along x-axis.

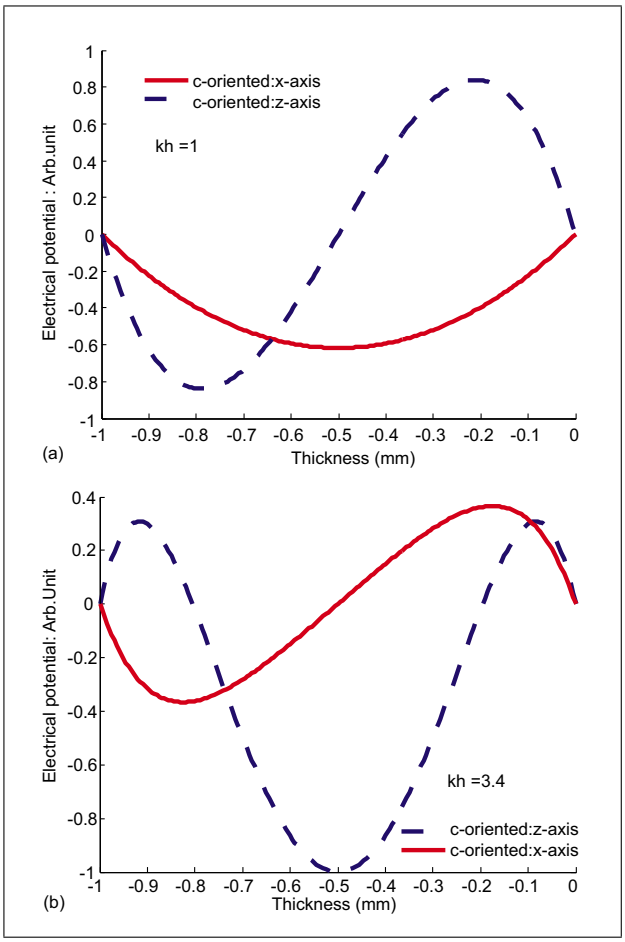

Figure 15. Electric potential of the S_0 mode (a) $kh = 1$ and (b) $kh = 3.4$, for electrically shorted circuit: dashed line: polarization along z-axis, solid line: polarization along x-axis.

eling. The study covered both types of polarization shorted and open circuit and multiple FGPM configurations, where the gradient coefficient has been varied significantly. The effects of the gradient coefficient on phase velocity, relative velocity shift and electromechanical coupling factor are plotted and discussed. The electromechanical coupling factor decreases substantially with the increases of the gradient factor ? for S_0 mode and vertical configuration. The largest electromechanical coupling factor very close to 6%, has been obtained in the case of homogeneous plate. Also the maximum of the electromechanical coupling factor shifts to higher frequencies when the gradient is increasing. The Peano-series method leads more easily to the profiles of the various components of the state vector, which shed light on the variations of the coupling factor. It was established that a mechanical displacement in a symmetric manner and parallel to the piezoelectric axis, is always associated with a high electromechanical coupling factor.

Acknowledgement

The authors are grateful for the funding provided to their laboratory by the Tunisian Ministry of Higher Education, Scientific Research. The authors would like to thank the anonymous reviewers for their valuable comments.

References

[1] S. G. Joshi, Y. Jin: Propagation of ultrasonic Lamb waves in piezoelectric plates. J. Appl. Phys. **70** (1991) 4113.

[2] F. Benmeddour, S. Grondel, J. Assaad, E. Moulin: Experimental study of the A0 and S0 Lamb waves interaction with symmetrical notches. Ultrasonics **49** (2009) 202–205.

[3] G. Wingqvist, L. Arapan, V. Yantchev, I. Katardjiev: A micromachined thermally compensated thin film Lamb wave resonator for frequency control and sensing applications. J. Micromech. Microeng. **19** (2009).

[4] X. Cao, F. InsuJeon: Calculation of propagation properties of Lamb waves in a functionally graded material (FGM) plate by power series technique. NDT&E International **44** (2011) 84–92.

[5] H. Liu, Z. B. Kuang, Z. M. Cai: Propagation of Bleustein-Gulyaev waves in a prestressed layered piezoelectric structures. Ultrasonics **41** (2003) 397–405.

[6] K. H. Chiu, J. H. Chen, H. R. Chen. Thin Solid Films **515** (2007) 4819–4825.

[7] I. Ben Salah, Y. Wali, M. H. Ben Ghozlen: Love waves in functionally graded piezoelectric materials by stiffness matrix method. Ultrasonic **51** (2011) 310–316.

[8] A. L. Shuvalov, E. Le Clezio, G. Feuillard: The state-vector formalism and the Peano-series solution for modelling

guided waves in functionally graded anisotropic piezoelectric plates. International Journal of Engineering Science **46** (2008) 929–947.

[9] C. Baron, S. Naili: Propagation of elastic waves in a fluid-loaded anisotropic functionally graded waveguide: Application to ultrasound characterization. J. Acoust. Soc. Am. **127** (2010) 1307–1317.

[10] C. Baron: Peano expansion of the matricant to study elastic wave propagation in continuously heterogeneous media (in French). Université Bordeaux 1.

[11] W. T. Thomson: Transmission of elastic waves through a stratified solid medium. Journal of Applied Physics **21** (1950) 89–93.

[12] N. A. Haskell: The dispersion of surface waves on multilayered media. Bulletin of the Seismological Society of America **43** (1953) 17–34.

[13] A. H. Fahmy, E. L. Alder: Propagation of acoustic waves in multilayers: a matrix description. Appl. Phys. Lett. **20** (1973) 495–497.

[14] E. L. Alder: SAW and pseudo SAW properties using matrix methods. IEEE Trans., Ferroelect., Freq. Cont. **41** (1994) 876–882.

[15] S. I. Rokhlin, L. Wang: Stable recursive algorithm for elastic wave propagation in layered anisotropic media: stiffness matrix method. J. Acoust. Soc. Am. **112** 822–834.